Molecular Imaging
Volume 16 : 1-11

DOI: 10.1177/1536012117711369
journals.sagepub.com/home/mix
SAGE

Imaging Neurotensin Receptor in Prostate Cancer With ^{64}Cu-Labeled Neurotensin Analogs

Huaifu Deng, MD[1,2], Hui Wang, PhD[1], He Zhang, MD[1,3], Mengzhe Wang, MS[1], Ben Giglio, PhD[1], Xiaofen Ma, MD[1,4], Guihua Jiang, MD[4], Hong Yuan, PhD[1], Zhanhong Wu, PhD[1], and Zibo Li, PhD[1]

Abstract

Introduction: Neurotensin receptor 1 (NTR-1) is expressed and activated in prostate cancer cells. In this study, we explore the NTR expression in normal mouse tissues and study the positron emission tomography (PET) imaging of NTR in prostate cancer models.

Materials and Methods: Three ^{64}Cu chelators (1, 4, 7, 10-tetraazacyclododecane-1, 4, 7, 10-tetraacetic acid [DOTA], 1,4,7-triazacyclononane-N,N′,N″-triacetic acid [NOTA], or AmBaSar) were conjugated to an NT analog. Neurotensin receptor binding affinity was evaluated using cell binding assay. The imaging profile of radiolabeled probes was compared in well-established NTR$^+$ HT-29 tumor model. Stability of the probes was tested. The selected agents were further evaluated in human prostate cancer PC3 xenografts.

Results: All 3 NT conjugates retained the majority of NTR binding affinity. In HT-29 tumor, all agents demonstrated prominent tumor uptake. Although comparable stability was observed, ^{64}Cu-NOTA-NT and ^{64}Cu-AmBaSar-NT demonstrated improved tumor to background contrast compared with ^{64}Cu-DOTA-NT. Positron emission tomography/computed tomography imaging of the NTR expression in PC-3 xenografts showed high tumor uptake of the probes, correlating with the in vitro Western blot results. Blocking experiments further confirmed receptor specificity.

Conclusions: Our results demonstrated that ^{64}Cu-labeled neurotensin analogs are promising imaging agents for NTR-positive tumors. These agents may help us identify NTR-positive lesions and predict which patients and individual tumors are likely to respond to novel interventions targeting NTR-1.

Keywords

neurotensin receptor 1 (NTR-1), prostate cancer, ^{64}Cu, positron emission tomography (PET)

Introduction

Malignant carcinoma of the prostate is the most frequently diagnosed noncutaneous malignancy and the second leading cause of cancer-related deaths among men in the United States.[1] Although antiandrogen therapy may be used to treat prostate cancers, in a number of cases, the tumor could become refractory and develop into a more aggressive neuroendocrine phenotype.[2-5] Recently, overexpression of NTRs was suggested to be responsible for prostate cancer progression and proliferation.[6,7] In advanced prostate cancer, NTRs were recruited as an alternative growth pathway in the absence of androgens.[8-10] In fact, prostate cancer could become enriched with (or entirely composed of) neuroendocrine cell clusters after long-term antiandrogen therapy.[2-5,7] Secreted by neuroendocrine-like prostate cells, neurotensin (NT) has numerous physiological effects predominantly

[1] Department of Radiology, Biomedical Research Imaging Center, University of North Carolina at Chapel Hill, Chapel Hill, NC, USA
[2] PET/CT Center, The First Affiliated Hospital of Guangzhou Medical University, Guangzhou, China
[3] Department of Radiology, Obstetrics and Gynecology Hospital, Fudan University, Shanghai, China
[4] Department of Medical Imaging, Provincial People's Hospital, Guangzhou, China

Submitted: 31/08/2016. Revised: 22/03/2017. Accepted: 26/04/2017.

Corresponding Authors:
Zibo Li, Department of Radiology, Biomedical Research Imaging Center, University of North Carolina at Chapel Hill, Chapel Hill, NC 27599, USA.
Email: zibo_li@med.unc.edu
Guihua Jiang, Department of Medical Imaging, Guangdong No. 2 Provincial People's Hospital, Guangzhou, China.
Email: jiangguihua1970@163.com

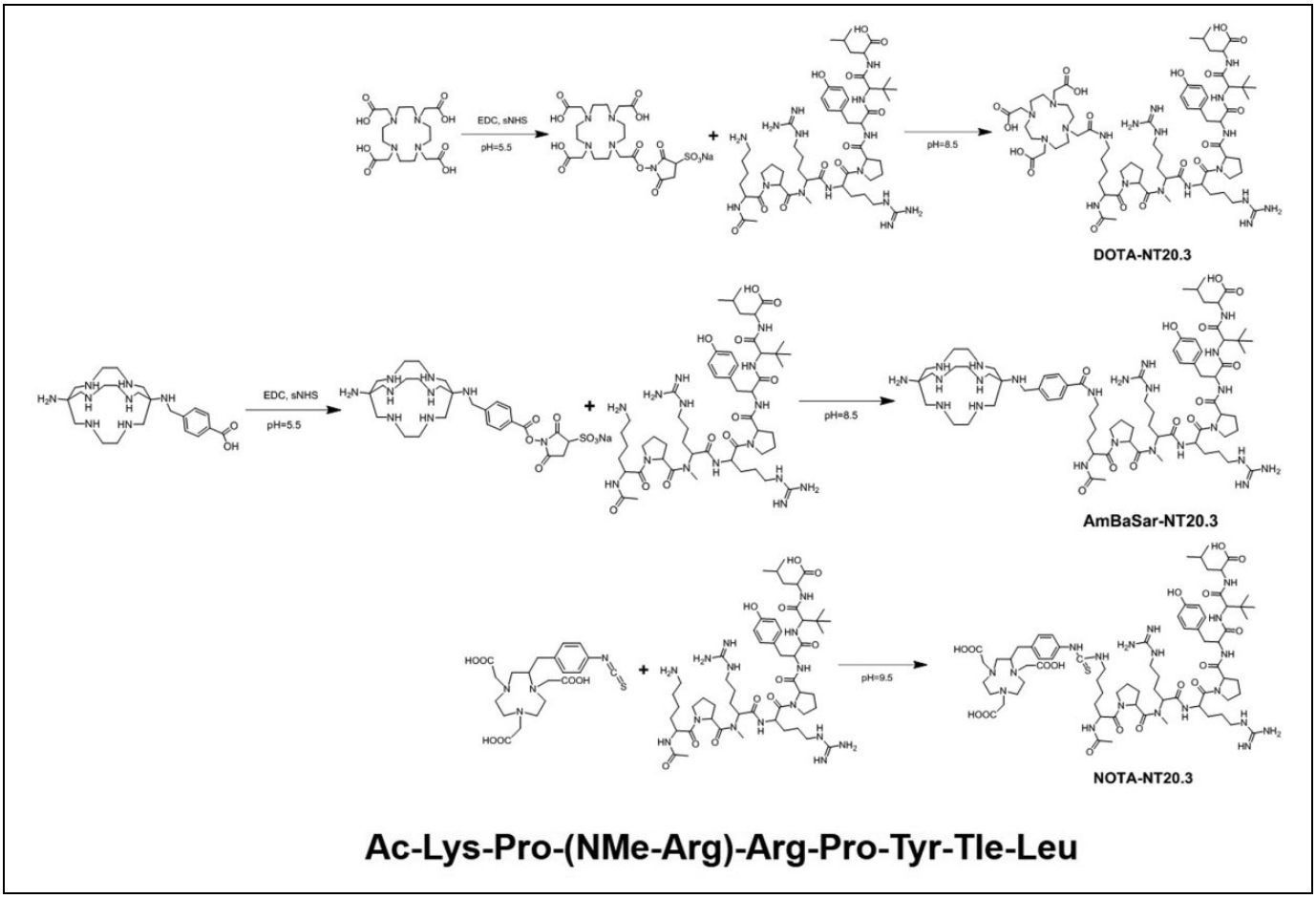

Scheme 1. Structures of 64Cu-AmBaSar-NT, 64Cu-DOTA-NT, and 64Cu-NOTA-NT.

mediated through its high-affinity receptor NTR-1. Neurotensin receptor 1 was found to be expressed and activated in aggressive prostate cancer cells but not in normal prostate epithelial cells.[7,11,12] Based on the important function of NTR-1, therapies (such as radiotherapy with radiolabeled NT analogs and chemotherapy with NTR-1 antagonists) focusing on this target have become potentially important components of prostate cancer treatment strategies. For example, inhibition of the NTR-1 and its downstream signaling selectively sensitizes prostate cancer to ionizing radiation.[13]

Clearly, the high incidence of NTR-1 in prostate cancer makes it a promising target for prostate cancer therapy and prognosis. The development of imaging agents to obtain NTR expression profiles of individual tumors may therefore lead to efficient early-stage diagnosis and customized treatment options for patients with prostate cancer. Because the native NT peptide gets metabolized rapidly in plasma by endogenous peptidases, various NT analogs have been developed to improve its in vivo stability. Several radiolabeled NT analogs were recently developed as a valuable tool for both imaging and therapy of NTR-positive tumors.[14-23] Copper-64 ($t_{1/2}$ = 12.7 hours) decays by β^+ (20%) and β^- emission (37%), as well as electron capture (43%), making it well suited for radiolabeling proteins, antibodies, and peptides, both for positron emission tomography (PET) imaging ($\beta+$) and therapy (β^+ and β^-).[24] It has been shown that the radiometal chelator could potentially have significant impact on in vivo imaging results. In this study, we focus on ^{64}Cu-labeled NT analog for the detection of NTR-positive tumors by PET imaging and evaluated the chelator effect on tumor imaging. We therefore conjugate 3 chelators (1, 4, 7, 10-tetraazacyclododecane-1, 4, 7, 10-tetraacetic acid [DOTA], 1,4,7-triazacyclononane-N,N′,N″-triacetic acid [NOTA], and AmBaSar) to NT20.3 analog [Ac-Lys-Pro-(NMe-Arg)-Arg-Pro-Tyr-Tle-Leu; abbreviated to NT below) radiolabeled with ^{64}Cu (Scheme 1) and evaluate their in vivo imaging capabilities. Receptor binding affinity of the 3 compounds was compared in well-established, NTR-positive human colon tumor (HT29) cells. Preliminary in vivo screening was then performed in HT29 mouse xenografts. The selected agent was further evaluated in vivo using human prostate cancer mouse xenograft models.

Materials and Methods

General

All chemicals and solvents were obtained from commercial sources and used without further purification. AmBaSar was synthesized by our research group according to literature-

reported procedure.[25] The DOTA, *p*-SCN-Bn-NOTA, was purchased from Macrocyclics, Inc. NT-Lys peptide (NT20.3) was purchased from CS Bio Co. ^{64}Cu was obtained from Washington University (St Louis, Missouri) and University of Wisconsin (Madison, Wisconsin). ^{64}Cu was produced using the ^{64}Ni (p, n) ^{64}Cu nuclear reaction and supplied in high-specific activity as $^{64}CuCl_2$ in 0.1 N HCl.

Synthesis of AmBaSar-, DOTA-, and NOTA-NT. AmBaSar (2.0 μmol) and DOTA (2.0 μmol) were added to the water solution of 1-ethyl-3-(3-dimethylaminopropyl)-carbodiimide (EDC, 1.7 μmol) and N-hydroxysulfosuccinimide (1.5 μmol), respectively. The pH of the mixture was adjusted with 0.1 N NaOH to pH 5.5, gently mixed and incubated between 20°C and 25°C for 30 minutes. Lys-NT (1.76 mg, 1.6 μmol) in 40 μL borate buffer (pH 8.5) was then added to the AmBaSar or DOTA solution. The reaction mixture stayed at 4°C overnight. For NOTA-NT, a mixture of *p*-SCN-Bn-NOTA (0.73 mg, 1.3 μmol) and Lys-NT (0.32 mg, 1.2 μmol) in 0.1 M sodium carbonate buffer (pH 9.5) was allowed to react for 20 hours at room temperature in the dark. The reaction mixtures were purified by high-performance liquid chromatography (HPLC). The retention time of AmBaSar-NT, DOTA-NT, and NOTA-NT on analytical HPLC is 15.3, 17.5, and 17.6 minutes, respectively. The products were confirmed by Q-TOF Liquid chromatography-mass spectrometry (LC-MS): AmBaSar-NT ($C_{74}H_{126}N_{23}O_{12}$, calculated $[MH]^+$: 1528.99, observed *m/z* 1529.01); DOTA-NT ($C_{68}H_{114}N_{19}O_{18}$, calculated $[MH]^+$: 1484.85, observed *m/z* 1484.63); and NOTA-NT ($C_{73}H_{118}N_{19}O_{17}S$, calculated $[MH]^+$: 1564.86, observed *m/z* 1564.82). The methods were as follows: The analyses were performed on a Waters (Milford, Massachusetts) Acquity Ultra Performance LC binary solvent manager coupled to a Diode array (PDA) detector and Waters (Micromass UK Limited, Manchester, United Kingdom) Q-TOF Premier. All the samples (10 μL) were injected into a Waters 50 × 2.1 mm ID, 1.7 μm Ethylene Bridged Hybrid C_{18} column and eluted using a 10-minute linear gradient starting from 100% water containing 0.1% formic acid and ending by 35% acetonitrile containing 0.1% formic acid at a flow rate of 0.5 mL/min. Positive electrospray ionization in V-mode with an extended dynamic range was used under the following conditions: capillary 3.5 kV, sampling cone 25 V, extraction cone 4.5 V, source temperature 100°C, and desolvation temperature 380°C. Two scan functions, MS and MS^E, in the mass range of 200 to 2000 Da, were performed simultaneously. The collision energy was set to 5 eV during the MS acquisition, and it was ramped from 10 to 35 eV during the MS^E acquisition.

Radiochemistry

All ^{64}Cu labeling reactions were performed using the same protocol.[20] In brief, $^{64}CuCl_2$ (74 MBq) was added to 15 μg AmBaSar-NT, DOTA-NT, and NOTA-NT conjugated in 0.1 N ammonium acetate (pH 5.5), respectively. The reaction mixture was kept at 37°C for 60 minutes. ^{64}Cu-labeled compounds were subsequently purified by analytical HPLC (Shimadzu Co, Ltd, Durham, North Carolina),using a Phenomenex Gemini C18 (Torrance, California). At a flow rate of 1 mL/min, the mobile phase was maintained at 95% solvent A (0.1% trifluoroacetic acid [TFA] in water) and 5% B (0.1% TFA in acetonitrile (MeCN]) from 0 to 2 minutes and was changed to 35% solvent A and 65% solvent B through 2 to 32 minutes. The UV absorbance was monitored at 280 nm. The radioactive peak containing the desired product was collected. After removal of the solvent by rotary evaporation, the conjugated peptide tracer was reconstituted in 1 × phosphate-buffered saline (PBS) for in vivo animal experiments after adjusting pH value to 7.0.

Cells and Animals

The human colon adenocarcinoma cell line HT-29, prostate cancer cell line PC-3, and LnCaP were obtained from the Tissue Culture Facility of UNC Lineberger Comprehensive Cancer Center. In brief, HT-29, PC-3, and LnCaP cells were cultured in McCoy's 5A, Dulbecco's Modified Eagle Medium: Nutrient Mixture F-12 (DMEM/F-12) Media, and Roswell Park Memorial Institute (RPMI) 1640, respectively, supplemented with 10% fetal bovine serum in a humidified atmosphere of 5% CO_2 at 37°C. When grown to 60% to 80% confluence, the cells were detached with 0.05% trypsin-EDTA for cell binding assay or animal tumor inoculation. Male/female *BALB*/c nude mice and NSG mice (NOD scid gamma, NOD.Cg-*Prkdc*^{scid} *Il2rg*^{tm1Wjl}/SzJ) of 4 to 6 weeks were purchased from Animal Study Facility of UNC–Chapel Hill. All work performed on animals were in accordance with and approved by UNC Institutional Animal Care and Use Committee. Specifically, PC 3 cells and HT29 cells (5×10^6) were subcutaneously injected into the shoulder of the male and female BALB/c nude mice, respectively (N = 7). LnCaP cells (10×10^6) were mixed with Matrigel at 1:1 volume ratio and subcutaneously injected into the shoulder of NSG mice (N = 3). The mice were used for small animal PET imaging studies when the tumor reached about 200 to 500 mm^3 in volume (3-4 weeks after inoculation of PC-3 cells and HT29 cells and 8-10 weeks after inoculation of LnCaP cells).

Cell Binding Assay

The in vitro NTR1 binding affinity of Lys-NT20.3, AmBaSar-NT20.3, DOTA-NT20.3, and NOTA-NT20.3 was assessed via competitive cell binding assays using ^{125}I-NT (8-13) (Perkin Elmer, Waltham, Massachusetts), as described previously.[22] In brief, binding assays were performed using 2×10^5 HT29 cells which are NTR positive[23] with 10^5 cpm of ^{125}I-NT in a total volume of 0.2 mL NTR binding buffer. Displacement curves were constructed by including various concentrations of unlabeled NT or newly synthesized NT-based probes (as indicated), and nonspecific binding was defined as that occurring in the blank well without cells. Incubations were performed at room temperature for 1 hour and stopped by washing the wells with ice-cold PBS (pH 7.4) twice and adding 1 N NaOH 300 μL into each well. The bound counts were measured using a γ-counter.

The best-fit 50% inhibitory concentration (IC_{50}) values for HT-29 cells were calculated by fitting the data with nonlinear regression using GraphPad Prism (GraphPad Software). Experiments were performed with quadruplicate samples.

Western Blots Analysis

Mouse normal organs and tumor xenografts were fractionated into small pieces, suspended in radioimmunoprecipitation assay buffer (RIPA) buffer containing 1× protease inhibitor cocktail which was diluted 10-fold from 2 mM AEBSF, 1 mM EDTA, 130 μM bestatin, 14 μM E-64, 1 μM leupeptin, and 0.3 μM aprotinin reconstituted in 100 mL of buffer as instructed by the manufacture (Sigma Aldrich) and broke down using a tissue homogenizer. The tissue samples were centrifuged at 12 000 rpm for 15 minutes at 4°C. Supernatants were collected and prepared for electrophoresis analysis. Cells were washed with cold PBS and lysed in RIPA buffer containing 1× protease inhibitor cocktail. Ten micrograms of tissue or cell lysates were separated by 4% to 12% NuPAGE gel followed by transfer to Polyvinylidene difluoride (PVDF) membrane. The NTR1 protein was probed with rabbit antihuman NTR1 polyclonal antibody (H-130; Santa Cruz Biotechnology) and visualized as previously described.[26] The β-actin was used as internal reference. Commercial available mouse cerebrum extract was used as NTR1-positive control and included in Western blot analysis to facilitate the identification of NTR1 band.

Biodistribution Study and Small Animal PET Imaging

Biodistribution was performed in nude mice bearing HT-29 adenocarcinoma xenografts. Animals were killed under inhalation anesthesia at 4 hours after injection of ~3.7 MBq of ^{64}Cu-AmBaSar-NT, ^{64}Cu-DOTA-NT, and ^{64}Cu-NOTA-NT respectively. Tissues and organs of interest were excised and weighed. Radioactivity in each excised specimen was measured using a γ counter; radioactivity uptake was expressed as percentage injected dose per gram (%ID/g). The mean uptake and corresponding standard deviation (SD) was calculated for each group of animals.

Positron emission tomography scans and image analysis were performed on prostate cancer models. In brief, each mouse bearing PC-3 or LnCaP xenograft was injected with approximately 3.7 MBq of ^{64}Cu-AmBaSar-NT, ^{64}Cu-DOTA-NT, or ^{64}Cu-NOTA-NT via the tail vein (n = 3/group). The same amount of activity was injected into the blocking group with unlabeled NT (10 mg/kg body weight) by the tail vein injection. The imaging data were collected at 1 and 4 hours postinjection (p.i.) using a small animal PET scanner (GE eXplore Vista), with the mice under anesthesia using isoflurane (5% for induction and 2% for maintenance in 100% O_2). The regions of interest (ROIs) were converted to counts per gram per minute based on the assumption of 1 g/mL tissue density. Dividing counts per gram per minute by injected dose gave the image ROI-derived %ID/g values. To investigate the blood half-life of ^{64}Cu-NOTA-NT, a 20-minute dynamic PET acquisition was then initiated prior to the administration of approximately 3.7 MBq in about 150 to 300 μL PBS via tail vein over 10 seconds. The list-mode dynamic PET data were reconstructed using OSEM algorithm with attenuation correction into the following dynamic frames (frames, time(s): 3,5; 3,15; 4,60; 5,180). The reconstructed images were composed of 14 transverse slices. The ROIs in the region corresponding to the Left ventricle blood pool (LVBP) were drawn in the last time frame of the dynamic image data in the transverse plane and time activity curves (TACs) generated for the LVBP for the 20-minute scan.

In Vitro and In Vivo Stability

After incubating in PBS at pH 7.5, the in vitro stability of ^{64}Cu-AmBaSar-NT, ^{64}Cu-DOTA-NT, and ^{64}Cu-NOTA-NT was analyzed by HPLC at 1- and 4-hour time point. For in vivo metabolic stability, the urine samples were collected and analyzed by HPLC at 30 minutes p.i.

Data Analysis

Quantitative data are expressed as mean (SD). Means were compared using one-way analysis of variance and Student *t* test (version 13.0; SPSS Inc, Chicago, Illinois). *P* values of less than 0.05 were considered statistically significant.

Results

Chemistry and Radiochemistry

The synthesis of ^{64}Cu-AmBaSar-NT, ^{64}Cu-DOTA-NT, and ^{64}Cu-NOTA-NT was performed according to reported methods. In the first step, the free carboxyl group on AmBaSar and DOTA was activated with EDC/Sulfo-NHS and then reacted with Lys-NT at pH 8.5. NOTA-NT was synthesized from the reaction with commercially available NOTA-SCN at higher pH. The AmBaSar-NT, DOTA-NT, and NOTA-NT were labeled with ^{64}Cu efficiently in 0.1 M NH_4OAc buffer within 60 minutes at 37°C. The specific activity of ^{64}Cu-AmBaSar-NT, ^{64}Cu-DOTA-NT, and ^{64}Cu-NOTA-NT was about 10.2 GBq/μmol. The decay-corrected yields of 3 tracers were all higher than 90%. The radiochemical purities of 3 tracers were all greater than 98.9% at 30 minutes after incubation in PBS. At 4 hours postincubation, ^{64}Cu-AmBaSar-NT and ^{64}Cu-DOTA-NT have a purity of greater than 96.8%, while ^{64}Cu-NOTA-NT has a purity of 93.7% (Figure 1).

Metabolic Stability Study

The metabolic stability of ^{64}Cu-AmBaSar-NT, ^{64}Cu-DOTA-NT, and ^{64}Cu-NOTA-NT was determined in collected mouse urine. We analyzed their urine metabolites, and 2 major metabolite peaks were found at 9- to 12- and 15- to 18-minute time point. Besides 2 major peaks, a small peak appearing at about 3.5 minutes was also observed consistently in both ^{64}Cu-

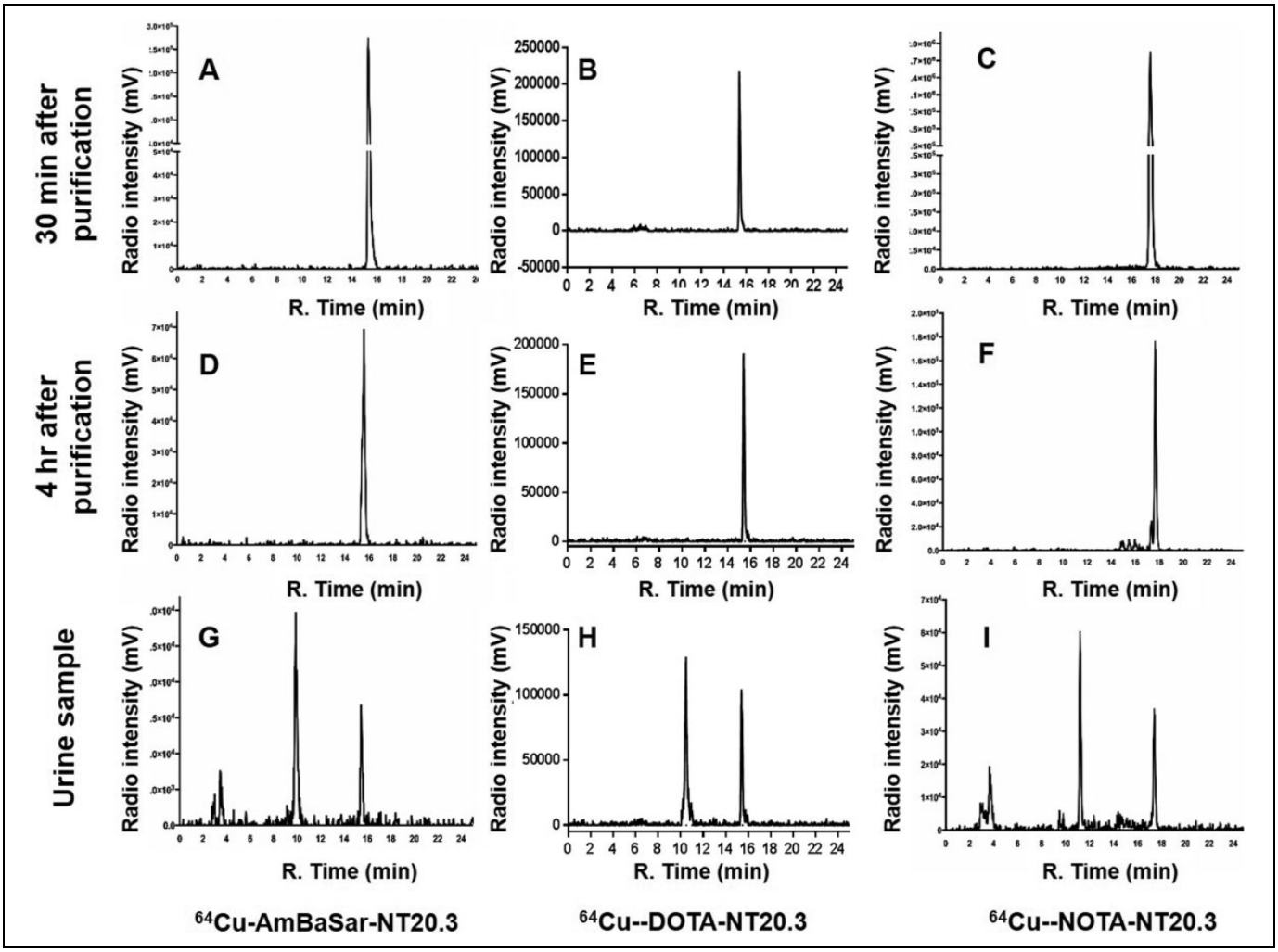

Figure 1. High-performance liquid chromatography (HPLC) radiochromatograms of 64Cu-AmBaSar-NT, 64Cu-DOTA-NT, and 64Cu-NOTA-NT at 30 minutes (A, B, C) and 4 hours (D, E, F) after purification and urine samples of 64Cu-AmBaSar-NT (G), 64Cu-DOTA-NT (H), and 64Cu-NOTA-NT (I) at 30 minutes postinjection.

AmBaSar-NT and ^{64}Cu-NOTA-NT tracer (Figure 1). These data suggest the peptide stability might play a dominant role here instead of chelator stability.

In Vitro Cell Binding Affinity

We compared the receptor binding affinity of AmBaSar-NT, DOTA-NT, and NOTA-NT with that of NT (8-13) using a competitive cell binding assay (Figure 2). All 3 conjugates inhibited the binding of ^{125}I-NT (8-13) to NTR-1 positive HT29 cells in a dose-dependent manner. The IC_{50} (the half maximal inhibitory concentration) values of AmBaSar-NT, DOTA-NT, and NOTA-NT were comparable to that of NT (8-13). The IC_{50} value for DOTA- NT, NOTA- NT, and AmBaSar-NT was 2.9 $\pm$ 1.2 nM, 3.0 $\pm$ 1.4 nM, and 4.8 $\pm$ 1.0 nM, respectively. The results demonstrated that AmBaSar, DOTA, and NOTA conjugation didn't significantly compromise receptor binding affinity to NTR1 of the Lys-NT peptide (2.4 $\pm$ 0.3 nM).

Biodistribution Studies

Biodistribution studies were performed in a group of HT-29 tumor–bearing mice at 4 hours after injection of ^{64}Cu-AmBaSar-NT, ^{64}Cu-DOTA-NT, or ^{64}Cu-NOTA-NT, respectively. HT29 tumor model was used for biodistribution study because it has relatively a high NTR1 expression level which will provide us clearer picture of tracer uptake in NTR-1-positive tumors. The tumor uptakes were 1.70 $\pm$ 0.44 %ID/g, 1.27 $\pm$ 0.24 %ID/g, and 1.64 $\pm$ 0.14 %ID/g at 4 hours p.i for ^{64}Cu-AmBaSar-NT, ^{64}Cu-DOTA-NT, and ^{64}Cu-NOTA-NT, respectively (Figure 3). These results showed that these 3 tracers had comparable tumor uptakes with ^{64}Cu-DOTA-NT-Cy5.5 and ^{64}Cu-neurotensin (8-13) cyclam derivatives.[22,27] The blood activity at 4 hours p.i. was low for all 3 tracers, and low radioactivity uptake was observed in most nontumor organs, except in kidney (6.71 $\pm$ 0.75 %ID/g, 4.28 $\pm$ 0.92 %ID/g, and 6.51 $\pm$ 0.63 %ID/g for ^{64}Cu-AmBaSar-NT, ^{64}Cu-DOTA-NT, and ^{64}Cu-NOTA-NT, respectively) and liver (1.41 $\pm$ 0.39 %ID/g, 0.42 $\pm$ 0.21 %ID/g, and 1.14 $\pm$ 0.09

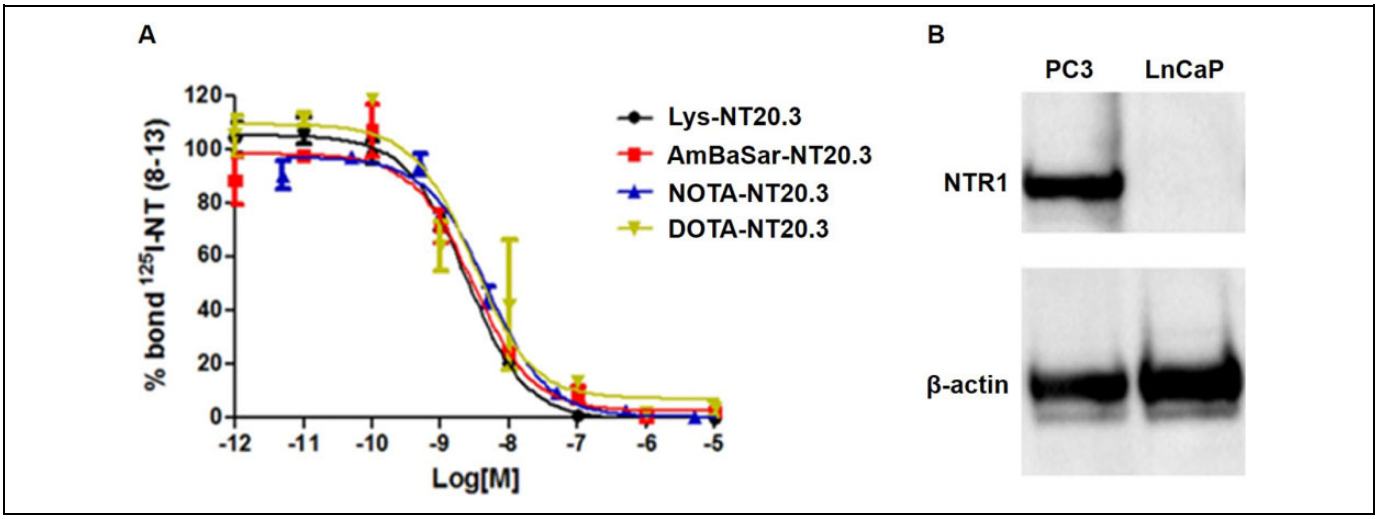

Figure 2. The cell binding affinity of 64Cu-AmBaSar-NT, 64Cu-DOTA-NT, and 64Cu-NOTA-NT and Western blot analysis of NTR1 expression in prostate tumors. A, Competitive cell binding assays of ^{125}I-NT (8-13) and AmBaSar-NT or Lys-NT in HT-29 cells. X-axis stands for the concentration of nonradiolabeled competitor. B, Western blot analysis of NTR1 expression in PC-3 (left) and LnCaP cells (right). β-actin was used as internal reference.

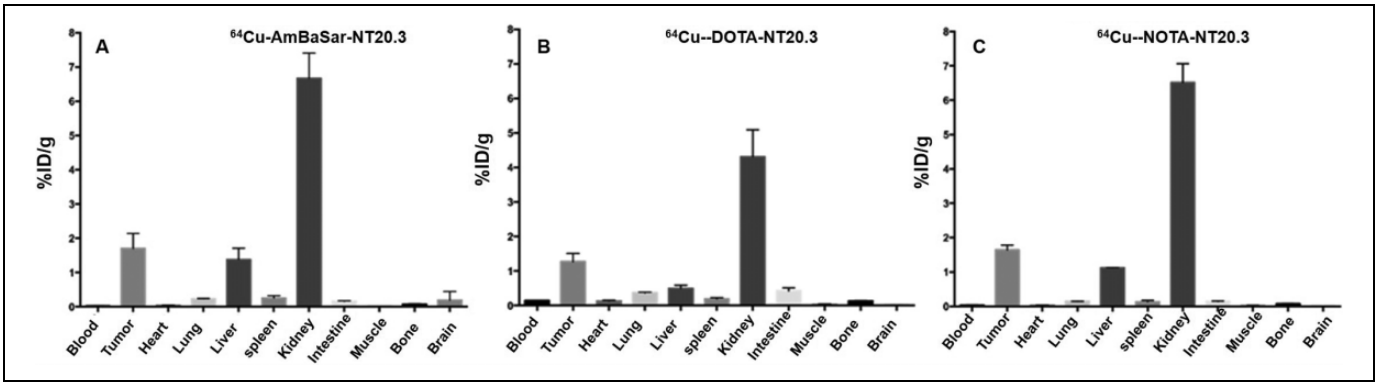

Figure 3. Biodistribution of 64Cu-AmBaSar-NT (A), 64Cu-DOTA-NT (B), and 64Cu-NOTA-NT (C) in mice bearing HT-29 xenograft at 4 hours postinjection (p.i.).

%ID/g for ^{64}Cu-AmBaSar-NT, ^{64}Cu-DOTA-NT, and ^{64}Cu-NOTA-NT, respectively). Interestingly, although we observed NTR1 expression in small intestine, which is consistent with literature report,[28] and ^{111}In-DOTA-NT20.3 showed 0.52 %ID/g ± 0.09 %ID/g uptake in small intestine with their contents at 3 hours p.i., we only observed comparable small intestine (contents emptied) uptake of ^{64}Cu-DOTA-NT at 4 hours p.i (Figure 3). The small intestine uptake of ^{64}Cu-AmBaSar-NT and ^{64}Cu-NOTA-NT was minimal, which may be explained by the chelator's effect on the distribution of radiotracers.

Small Animal Imaging in Prostate Cancer Models

Since the NTR-1 binding capability of the radiotracers has been confirmed in HT29 tumor model, we further tested the in vivo tumor-targeting properties of ^{64}Cu-AmBaSar-NT, ^{64}Cu-DOTA- NT, and ^{64}Cu-NOTA-NT in prostate cancer xenografts. As shown in Figure 4, the PC-3 tumors (NTR1 positive) were clearly visualized with high tumor-to-background contrast in all 3 groups. The ROI analysis on PET images shows that the tumor uptake was 1.21 ± 0.12 %ID/g (^{64}Cu-AmBaSar-NT), 1.18 ± 0.24 %ID/g (^{64}Cu-DOTA-NT), and 1.48 ± 0.34 %ID/g (^{64}Cu-NOTA-NT) at 1 hour p.i., respectively. The tumor uptake slightly increased to 1.77 ± 0.33 %ID/g, 1.48 ± 0.34 %ID/g, and 1.81 ± 0.49 %ID/g at 4 hours p.i. for PC-3 xenograft tumors (Figure 4A-C). The highest uptake for all 3 tracers was observed in kidneys (7.31 ± 0.63 %ID/g, 6.78 ± 0.83 %ID/g, and 6.35 ± 0.74 %ID/g at 1 hour p.i.; and 6.11 ± 0.90 %ID/g, 5.15 ± 0.76 %ID/g, and 4.91 ± 0.45 %ID/g at 4 hours p.i.). However, ^{64}Cu-AmBaSar-NT had the highest liver uptake (1.56 ± 0.13 %ID/g at 1 hour p.i.) among the 3 tracers, followed by ^{64}Cu-NOTA-NT and ^{64}Cu-DOTA-NT (0.46 ± 0.08 %ID/g and 0.42 ± 0.14 %ID/g at 1 hour p. i.). The other normal organs had relatively low uptake in all 3 groups (Figure 4).

In order to confirm target specificity, ^{64}Cu-NOTA-NT was coinjected with unlabeled NT (10 mg/kg body weight) via tail

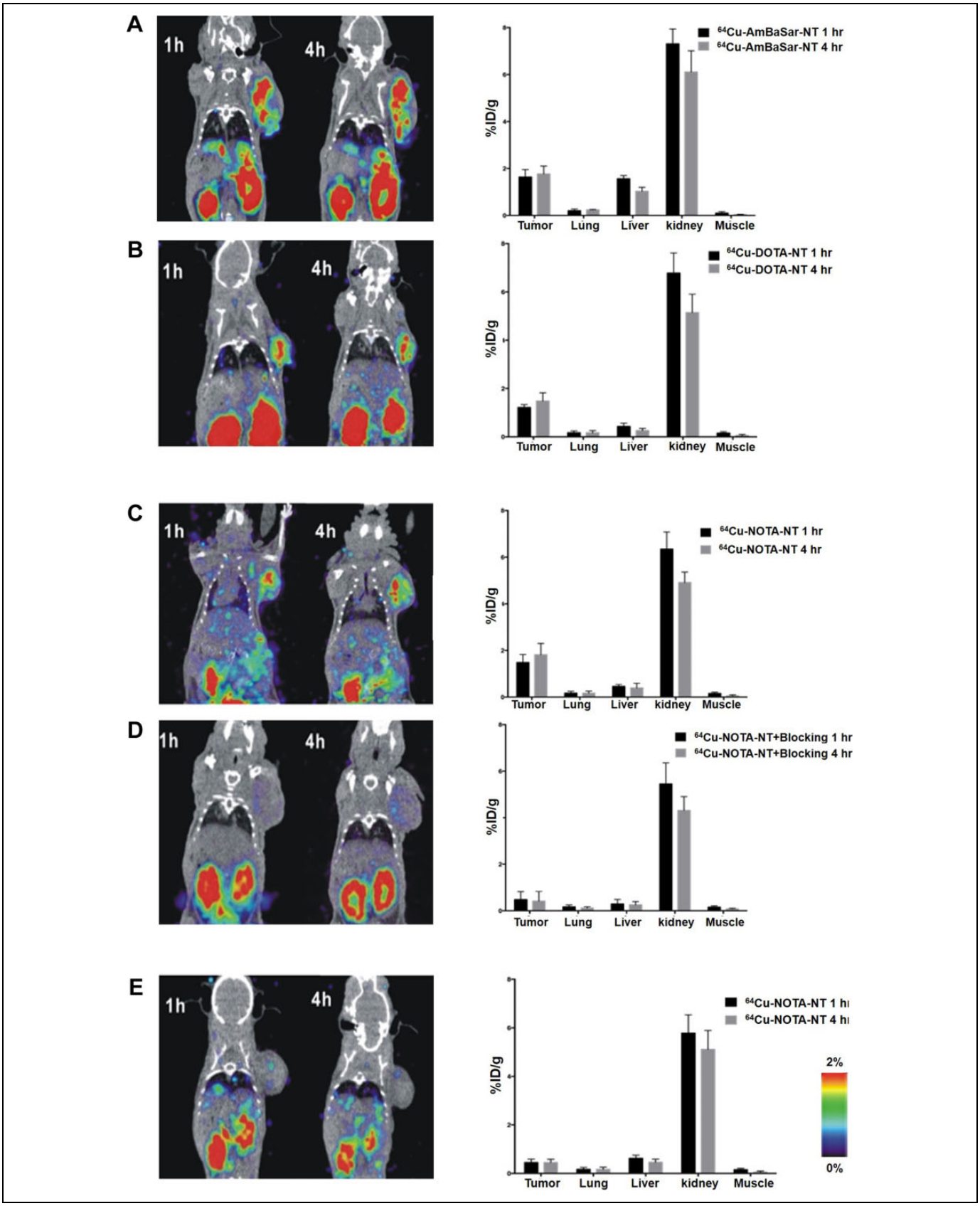

Figure 4. Representative positron emission tomography (PET) images in PC-3 xenografts. The representative PET images and quantitative analysis results of PC-3 tumor-bearing mice at 1 and 4 hours after injection of 64Cu-AmBaSar-NT (A), 64Cu-DOTA-NT (B), 64Cu-NOTA-NT (C), blocking group (D), and LnCaP tumor-bearing mice (E).

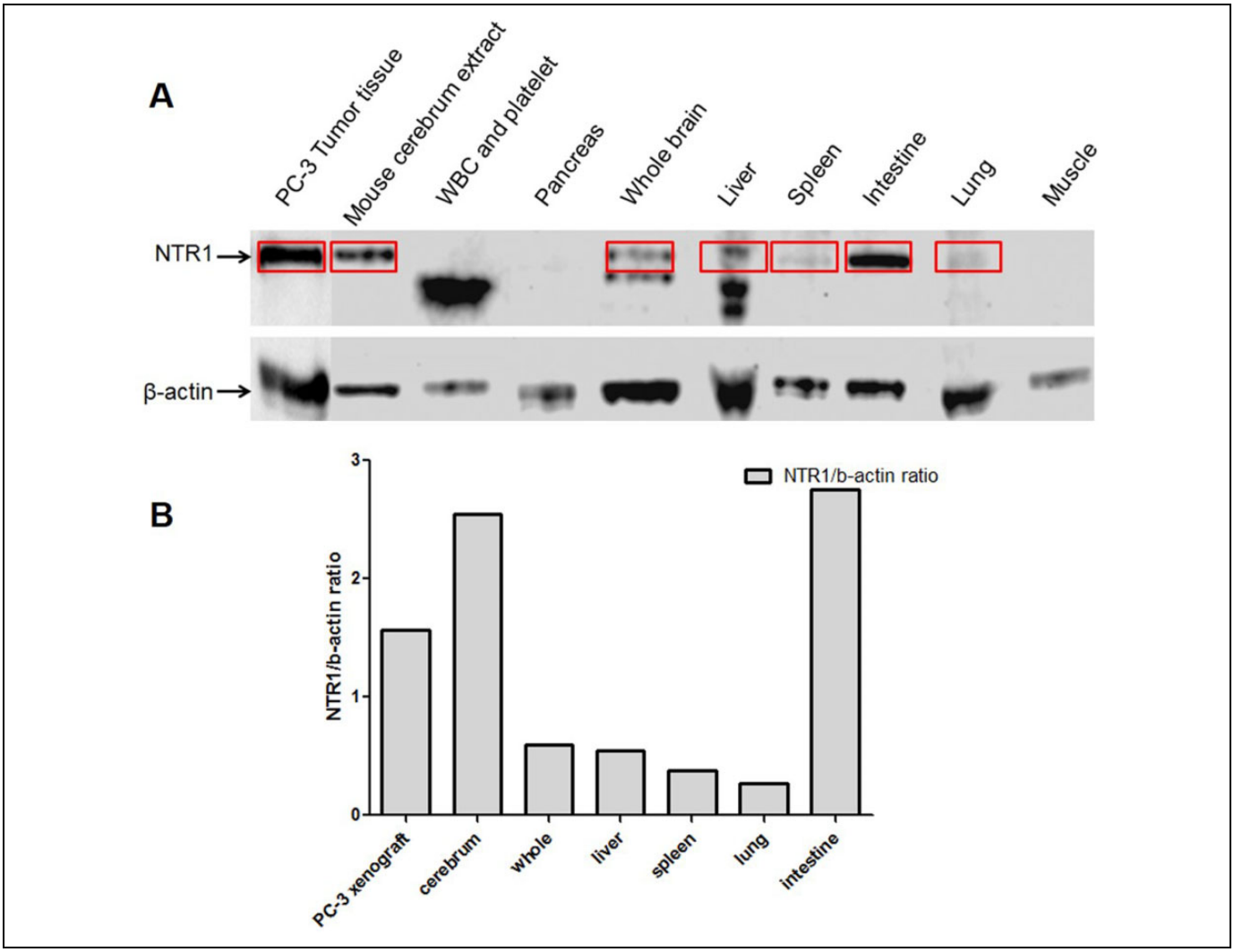

Figure 5. Neurotensin receptor 1 (NTR-1) expression profiling. A, Western blot analysis of NTR-1 expression in normal mouse organs and PC-3 xenograft. B, Semi-quantitative analysis of Western blot results.

vein in PC3 tumor-bearing mice (n = 3). As shown in Figure 4D, the tumor uptake was successfully reduced from 1.48 ± 0.34 %ID/g to 0.52 ± 0.29 %ID/g at 1 hour p.i. and from 1.81 ± 0.49 %ID/g to 0.49 ± 0.35 %ID/g at 4 hours p.i. However, the accumulation of ^{64}Cu-NOTA-NT in other major organs did not change significantly. The kidney accumulation was 5.48 ± 0.98 %ID/g at 1 hour and 4.23 ± 0.68 %ID/g at 4 hours after blocking (vs 6.35 ± 0.74 %ID/g at 1 hour and 4.91 ± 0.45 %ID/g at 4 hours p.i. without blocking); the liver accumulation was 0.23 ± 0.05 %ID/g after blocking versus 0.46 ± 0.08 %ID/g without blocking at 1 hour. These results demonstrated that tumor uptake of ^{64}Cu-NOTA-NT was mediated by active interaction between NT and NTR1 receptors overexpressed in PC3 tumors.

Using dynamic PET of mouse heart in vivo, we evaluated the blood half-life of ^{64}Cu-NOTA-NT (Supplementary Figure 3). The ROIs are shown in the blood and the myocardium in the last time frame. The ROI drawn in the last time frame was used to obtain TACs for the blood from the dynamic PET data. The blood levels of ^{64}Cu-NOTA-NT reached peak rapidly after injection, which was 26.77% of injected dose at 15 seconds p.i. Then the blood level of activity decreases rapidly to plateau. At the end of 20-minute dynamic scans, the blood levels of ^{64}Cu-NOTA-NT were 1.91 %ID/g.

The NTR1 Expression in Cell Culture, Mouse Normal Organs, and PC-3 Xenograft

Western blot analysis of the in vitro cultured PC-3 and LnCaP tumor cells showed that the PC-3 cells are NTR1 positive, while LnCaP cells have low NTR1 expression. In PC-3 tumor-bearing mouse, NTR1 expression on normal organs was also studied. As shown in Figure 5, NTR was mainly observed in intestine, cerebrum, and PC-3 tumor. The integrated optical density (IOD) of well-defined NTR1 bands and corresponding β-actin bands were analyzed semi-quantitatively, and the ratios between IODs of NTR1 and β-actin of major organs were calculated. The results showed that the NTR1 expression level

was highest in intestine with NTR1/β-actin ratio of 2.75, followed by cerebrum with NTR1/β-actin ratio of 2.55. The NTR1 expression levels of PC-3 xenograft were high, with NTR1/β-actin ratio of 1.57 (Figure 5B). In most other organs, including spleen, liver, lung, pancreas, muscle, white blood cell, and kidneys (Supplementary Figure 2B), NTR1 protein was either very low or not detected in our experiment.

Discussion

Neurotensin and its cognate receptor (NTR1) are neuropeptide receptor complexes frequently upregulated during the neoplastic process. Neurotensin is a 13-amino acid peptide previously recognized for its distribution along the gastrointestinal tract. The effects of NT are mediated by binding to 3 NT receptors NTR-1, -2, and -3. The peripheral functions of NT are mainly mediated through its interaction with NTR1, a high-affinity receptor coupled to a Gq/G11 protein.[29] Several reports implicate NTR1 in numerous detrimental functions linked to neoplastic progression of several cancer types, including pancreatic, prostate, colon, lung, and head and neck cancers.[9,30-32,33] Because overexpression of NTRs was suggested to be responsible for prostate cancer progression and proliferation,[6,7] we investigated using PET agents for NTR1 imaging recently. We first performed Western blots of NTR expression on LnCaP cell (androgen dependent) and PC3 cell (androgen independent). Indeed, the androgen-independent PC3 has much higher NTR expression than LnCaP as shown in Figure 2.

^{18}F-labeled agent is good for imaging applications and we have reported ^{18}F-labeled probe for NTR imaging previously.[21] However, radiolabeling NT ligand with ^{18}F requires multiple steps, which is more labor intensive and time-consuming. Different from ^{18}F-labeled agent, the radiometal-labeled analog allows seamless integration of imaging with radionuclide-based therapy (eg, Cu67- or Y90-based therapy). Therefore, in this study, we aim to evaluate chelator effect on NT-based PET tracers. Our ultimate goal is to develop the corresponding theranostic platform targeting NTR. The ^{68}Ga-labeled NT did not perform better than ^{64}Cu-labeled NT agent (data did not shown here) due to its higher positron energy (Emax = 1899 keV for ^{68}Ga and 653 KeV for ^{64}Cu). The higher positron energy would lead to decreased resolution on PET imaging. Indeed, the advantage of ^{68}Ga is attributed to its generator-based property (no need to have cyclotron on site). In addition, in our report, we compared different chelators, such as DOTA, NOTA, and AmBaSar for ^{64}Cu-labeling of NT, further optimized the radiosynthesis of NT-based PET tracers. Our research complement with what has been done in the literature.

It is well-known that the radiometal chelators could have significant effect on probe distribution in vivo.[34-36] Therefore, in this report, 3 radiometal chelators are conjugated to NT peptides (DOTA-NT, NOTA-NT, and AmBaSar-NT) aiming to select the most potent one for in vivo imaging applications. After conjugation, cell binding assay confirmed that addition of the chelate on the C-terminal lysine has minimal effect on NTR binding capacity. We then moving forward to study the impact of chelators on in vivo imaging result. Side-by-side comparison of 3 NT agents was performed using the well-established NTR-positive HT29 tumor. Based on the biodistribution study, all 3 tracers demonstrated prominent tumor uptake. The major uptake organ is kidney followed by liver. For unknown reason, DOTA-NT demonstrated slightly higher overall background uptake compared with NOTA-NT and AmBaSar-NT. All 3 agents demonstrated reasonable stability in vitro and comparable stability profile in urine sample. A major metabolite was observed at 11 minutes, which may be mainly caused by the decomposition of lys-NT peptide instead of demetalation from the chelators. We also compared the ^{64}Cu-labeled NT with ^{18}F-labeled NT. Both ^{18}F-labeled NT and ^{64}Cu-labeled NT showed rapid clearance from tumor-bearing mice. The ^{64}Cu-labeled NT analog in this study showed higher kidney accumulation as compared ^{18}F-DEG-VS-NT.[21] However, ^{64}Cu-labeled NT also exhibited higher tumor uptake than ^{18}F-DEG-VS-NT at later time point (1.54 %ID/g) at 4 hours p.i., as demonstrated in biodistribution study in HT29 xenografts.[21] The high kidney retention observed in this study may be caused by either demetalation or decomposition of Lys-NT. The exact mechanisms are not fully understood at the current stage. Nonetheless, for future radiotherapy application, efforts should be taken to reduce the kidney retention and potential nephrotoxicity. In order to reduce the renal accumulation of radiolabeled polypeptides, rational approaches should be explored including modifying the net charges of peptides and the blockage of renal reabsorption of polypeptides by basic amino acids and other reagents such as Gelofusine. Another aspect of future effort could be focused on using renal brush border enzyme-cleavable linkages to reduce renal uptake. For example, both glycyl-L-lysine linker and the newly developed glycyl-L-tyrosine linker could be used for this purpose.[37-39]

Because no obvious difference was observed on HT-29 tumor model, we then focused on prostate cancer and evaluated the PET imaging capability with ^{64}Cu-DOTA-NT, ^{64}Cu-NOTA-NT, and ^{64}Cu-AmBaSar-NT. As shown in Figure 4, all 3 agents could clearly visualize PC-3 tumor at 1 and 4 hours p.i. with good tumor-to-background contrast. Clearly, different chelators did not cause significant difference on tumor uptake here. In order to confirm target specificity, ^{64}Cu-NOTA-NT was coinjected with unlabeled NT peptide for blocking experiment. The results showed that tumor uptake of ^{64}Cu-NOTA-NT was successfully blocked by unlabeled NT peptide, which demonstrated that the tumor uptake of ^{64}Cu-NOTA-NT was mediated by receptor-specific binding. LnCaP cell expresses low NTR based on Western blot result. Consistently, LnCaP tumor did not demonstrate significant tracer uptake as expected.

In addition to tumor lesion, one potential concern would be the background uptake in normal organs. In situ hybridization studies revealed that the levocabastine low-affinity NT receptor (NTS_1) was mainly expressed in the hippocampus, in the piriform cortex, and also in the cerebellar cortex.[40] It has also been reported that NTR1-expressing cells are present in normal mucosa of the human colon.[41,42] Although Western blot

showed that small intestine has highest NTR1 protein expression, high uptake in small intestine was not observed in our study and others, which could be attributed to blood supply limitation and the possible effect of chelators. Whole brain also has high NTR1 protein expression, which was consistent with literature report.[43] However, we did not see significant brain uptake possibly due to blood–brain barrier. The NTR1 messenger RNA (mRNA) has been shown to be expressed by human B-cell lines.[43,40] However, our Western blot did not detect the NTR1 protein in whole blood cells and platelets. This discrepancy may be explained by the fact that mRNA of NTR1 may not be translated to NTR1 protein. Overall, the restricted NTR expression profile makes it a promising target for imaging and therapy applications. We would also like to point out that, unlike ^{18}F-labeled cys-NT_{mut},[21] the ^{64}Cu-labeled NT analogs demonstrated overall slower clearance especially at kidneys, which could be the dose-limiting organ. Whether this difference is caused by peptide sequence (2 different NTs) or by the nature of radioisotopes still needs to be determined. Although our NTR targeted agents could provide good tumor imaging contrast, the tumor uptakes of these probes in general are not high. Multimerization can improve affinity, enhance stability, and extend in vivo half-life of peptides. This multimeric approach may also be a valid approach for NTR imaging in future studies.

Conclusion

In summary, ^{64}Cu-DOTA-NT, ^{64}Cu-NOTA-NT, and ^{64}Cu-AmBaSar-NT were developed as promising imaging agents for NTR-positive tumors. Despite different chelators are used, 3 PET agents demonstrated comparable tumor imaging capability in vivo. These agents may play an important role in identifying NTR-positive lesions and predicting which patients and individual tumors are likely to respond to novel interventions targeting NTR-1.

Authors' Note

Huaifu Deng, Hui Wang, and He Zhang were contributed equally to this article.

Declaration of Conflicting Interests

The author(s) declared no potential conflicts of interest with respect to the research, authorship, and/or publication of this article.

Funding

The author(s) disclosed receipt of the following financial support for the research, authorship, and/or publication of this article: This work was supported by P30-CA016086-35-37 (NCI), the American Cancer Society (12199ss1-MRSG-12-034-01-CCE), NC TraCS (2KR631408), UNC Chapel Hill Department of Radiology and BRIC, and Chinese National Natural Science Foundation (No. 81201695) and China Scholarship Funding.

Supplementary Material

The supplements for the article are available online.

References

1. Jemal A, Siegel R, Ward E, Murray T, Xu J, Thun MJ. Cancer statistics, 2007. *CA Cancer J Clin*. 2007;57(1):43–66.
2. Falkmer S, Askensten U, Grimelius L, Abrahamsson PA. Cytochemical markers and DNA content of neuroendocrine cells in carcinoma of the prostate gland during tumour progression. *Acta Histochem Suppl*. 1990;38:127–132.
3. Huang J, Wu C, diSant'Agnese PA, Yao JL, Cheng L, Na Y. Function and molecular mechanisms of neuroendocrine cells in prostate cancer. *Anal Quant Cytol Histol*. 2007;29(3):128–138.
4. Oesterling JE, Hauzeur CG, Farrow GM. Small cell anaplastic carcinoma of the prostate: a clinical, pathological and immunohistological study of 27 patients. *J Urol*. 1992;147(3 pt 2):804–807.
5. Lee LF, Guan J, Qiu Y, Kung HJ. Neuropeptide-induced androgen independence in prostate cancer cells: roles of nonreceptor tyrosine kinases Etk/Bmx, Src, and focal adhesion kinase. *Mol Cell Biol*. 2001;21(24):8385–8397.
6. Arrighi N, Bodei S, Zani D, et al. Nerve growth factor signaling in prostate health and disease. *Growth Factors*. 2010;28(3):191–201.
7. Swift SL, Burns JE, Maitland NJ. Altered expression of neurotensin receptors is associated with the differentiation state of prostate cancer. *Cancer Res*. 2010;70(1):347–356.
8. Abrahamsson PA, Wadstrom LB, Alumets J, Falkmer S, Grimelius L. Peptide-hormone- and serotonin-immunoreactive tumour cells in carcinoma of the prostate. *Pathol Res Pract*. 1987;182(3):298–307.
9. Sehgal I, Powers S, Huntley B, Powis G, Pittelkow M, Maihle NJ. Neurotensin is an autocrine trophic factor stimulated by androgen withdrawal in human prostate cancer. *Proc Natl Acad Sci U S A*. 1994;91(11):4673–4677.
10. Seethalakshmi L, Mitra SP, Dobner PR, Menon M, Carraway RE. Neurotensin receptor expression in prostate cancer cell line and growth effect of NT at physiological concentrations. *Prostate*. 1997;31(3):183–192.
11. Amorino GP, Deeble PD, Parsons SJ. Neurotensin stimulates mitogenesis of prostate cancer cells through a novel c-Src/Stat5b pathway. *Oncogene*. 2007;26(5):745–756.
12. Elek J, Pinzon W, Park KH, Narayanan R. Relevant genomics of neurotensin receptor in cancer. *Anticancer Res*. 2000;20(1A):53–58.
13. Valerie NC, Casarez EV, Dasilva JO, et al. Inhibition of neurotensin receptor 1 selectively sensitizes prostate cancer to ionizing radiation. *Cancer Res*. 2011;71(21):6817–6826.
14. Bergmann R, Scheunemann M, Heichert C, et al. Biodistribution and catabolism of (18)F-labeled neurotensin(8-13) analogs. *Nucl Med Biol*. 2002;29(1):61–72.
15. Teodoro R, Faintuch BL, Nunez EG, Queiroz RG. Neurotensin(8-13) analogue: radiolabeling and biological evaluation using different chelators. *Nucl Med Biol*. 2011;38(1):113–120.
16. Buchegger F, Bonvin F, Kosinski M, et al. Radiolabeled neurotensin analog, 99mTc-NT-XI, evaluated in ductal pancreatic adenocarcinoma patients. *J Nucl Med*. 2003;44(10):1649–1654.
17. Zhang K, An R, Gao Z, Zhang Y, Aruva MR. Radionuclide imaging of small-cell lung cancer (SCLC) using 99mTc-labeled neurotensin peptide 8-13. *Nucl Med Biol*. 2006;33(4):505–512.

18. Garcia-Garayoa E, Blauenstein P, Blanc A, Maes V, Tourwe D, Schubiger PA. A stable neurotensin-based radiopharmaceutical for targeted imaging and therapy of neurotensin receptor-positive tumours. *Eur J Nucl Med Mol Imaging*. 2009;36(1): 37–47.
19. de Visser M, Janssen PJ, Srinivasan A, et al. Stabilised 111In-labelled DTPA- and DOTA-conjugated neurotensin analogues for imaging and therapy of exocrine pancreatic cancer. *Eur J Nucl Med Mol Imaging*. 2003;30(8):1134–1139.
20. Wu Z, Liu S, Nair I, et al. (64)Cu labeled sarcophagine exendin-4 for microPET imaging of glucagon like peptide-1 receptor expression. *Theranostics*. 2014;4(8):770–777.
21. Wu Z, Li L, Liu S, et al. Facile preparation of a thiol-reactive 18F-labeling agent and synthesis of 18F-DEG-VS-NT for PET imaging of a neurotensin receptor-positive tumor. *J Nucl Med*. 2014;55(7):1178–1184.
22. Deng H, Wang H, Wang M, Li Z, Wu Z. Synthesis and evaluation of 64Cu-DOTA-NT-Cy5.5 as a dual-modality PET/fluorescence probe to image neurotensin receptor-positive tumor. *Mol Pharm*. 2015;12(8):3054–3061.
23. Alshoukr F, Prignon A, Brans L, et al. Novel DOTA-neurotensin analogues for 111In scintigraphy and 68Ga PET imaging of neurotensin receptor-positive tumors. *Bioconjug Chem*. 2011;22(7): 1374–1385.
24. Kumar R, Dhanpathi H, Basu S, Rubello D, Fanti S, Alavi A. Oncologic PET tracers beyond [(18)F]FDG and the novel quantitative approaches in PET imaging. *Q J Nucl Med Mol Imaging*. 2008;52(1):50–65.
25. Liu S, Li D, Huang CW, et al. The efficient synthesis and biological evaluation of novel bi-functionalized sarcophagine for (64)cu radiopharmaceuticals. *Theranostics*. 2012;2(6):589–596.
26. Gao H, Kiesewetter DO, Zhang X, et al. PET of glucagonlike peptide receptor upregulation after myocardial ischemia or reperfusion injury. *J Nucl Med*. 2012;53(12):1960–1968.
27. Rohrich A, Bergmann R, Kretzschmann A, et al. A novel tetrabranched neurotensin(8-13) cyclam derivative: synthesis, 64Cu-labeling and biological evaluation. *J Inorg Biochem*. 2011;105(6): 821–832.
28. Bakirtzi K, West G, Fiocchi C, Law IK, Iliopoulos D, Pothoulakis C. The neurotensin-HIF-1alpha-VEGFalpha axis orchestrates hypoxia, colonic inflammation, and intestinal angiogenesis. *Am J Pathol*. 2014;184(12):3405–3414.
29. Martin S, Navarro V, Vincent JP, Mazella J. Neurotensin receptor-1 and -3 complex modulates the cellular signaling of neurotensin in the HT29 cell line. *Gastroenterology*. 2002; 123(4):1135–1143.
30. Shimizu S, Tsukada J, Sugimoto T, et al. Identification of a novel therapeutic target for head and neck squamous cell carcinomas: a role for the neurotensin-neurotensin receptor 1 oncogenic signaling pathway. *Int J Cancer*. 2008;123(8):1816–1823.
31. Thomas RP, Hellmich MR, Townsend CM Jr, Evers BM. Role of gastrointestinal hormones in the proliferation of normal and neoplastic tissues. *Endocr Rev*. 2003;24(5):571–599.
32. Yamada M, Ohata H, Momose K, Richelson E. Pharmacological characterization of SR 48692 sensitive neurotensin receptor in human pancreatic cancer cells, MIA PaCa-2. *Res Commun Mol Pathol Pharmacol*. 1995;90(1):37–47.
33. Sethi T, Langdon S, Smyth J, Rozengurt E. Growth of small cell lung cancer cells: stimulation by multiple neuropeptides and inhibition by broad spectrum antagonists in vitro and in vivo. *Cancer Res*. 1992;52(9 suppl):2737s–2742s.
34. Dale AV, An GI, Pandya DN, et al. Synthesis and evaluation of new generation cross-bridged bifunctional chelator for (64)Cu Radiotracers. *Inorg Chem*. 2015;54(17):8177–8186.
35. Litau S, Seibold U, Vall-Sagarra A, Fricker G, Wangler B, Wangler C. Comparative assessment of complex stabilities of radiocopper chelating agents by a combination of complex challenge and in vivo experiments. *ChemMedChem*. 2015; 10(7):1200–1208.
36. Wu N, Kang CS, Sin I, et al. Promising bifunctional chelators for copper 64-PET imaging: practical (64)Cu radiolabeling and high in vitro and in vivo complex stability. *J Biol Inorg Chem*. 2016; 21(2):177–184.
37. Huang CW, Li Z, Conti PS. In vivo near-infrared fluorescence imaging of integrin alpha2beta1 in prostate cancer with cell-penetrating-peptide-conjugated DGEA probe. *J Nucl Med*. 2011;52(12):1979–1986.
38. Akizawa H, Imajima M, Hanaoka H, Uehara T, Satake S, Arano Y. Renal brush border enzyme-cleavable linkages for low renal radioactivity levels of radiolabeled antibody fragments. *Bioconjug Chem*. 2013;24(2):291–299.
39. Uehara T, Koike M, Nakata H, et al. Design, synthesis, and evaluation of [188Re]organorhenium-labeled antibody fragments with renal enzyme-cleavable linkage for low renal radioactivity levels. *Bioconjug Chem*. 2007;18(1):190–198.
40. Kleczkowska P, Lipkowski AW. Neurotensin and neurotensin receptors: characteristic, structure-activity relationship and pain modulation—a review. *Eur J Pharmacol*. 2013;716(1-3):54–60.
41. Law IK, Bakirtzi K, Polytarchou C, et al. Neurotensin-regulated miR-133alpha is involved in proinflammatory signalling in human colonic epithelial cells and in experimental colitis. *Gut*. 2015;64(7):1095–1104.
42. Zhao D, Bakirtzi K, Zhan Y, Zeng H, Koon HW, Pothoulakis C. Insulin-like growth factor-1 receptor transactivation modulates the inflammatory and proliferative responses of neurotensin in human colonic epithelial cells. *J Biol Chem*. 2011;286:6092–6099.
43. Choi SY, Chae HD, Park TJ, Ha H, Kim KT. Characterization of high affinity neurotensin receptor NTR1 in HL-60 cells and its down regulation during granulocytic differentiation. *Br J Pharmacol*. 1999;126(4):1050–1056.